Design and Control of an Underactuated Finger Exoskeleton for Assisting Activities of Daily Living

Houcheng Li, Long Cheng, Ning Sun, and Ran Cao

***Abstract*—In this article, a novel underactuated finger exoskeleton is designed to assist grasping tasks for the elderly with weak muscle strength. In mechanical design, the human finger's phalanges and joints are considered as part of the kinematic chains to realize the human-robot kinematic compatibility. The proposed finger exoskeleton achieves the finger preshaping and grasps objects with generic shapes. The proposed exoskeleton is both actively and passively backdriveable. Moreover, the weight of the wearable part of the proposed exoskeleton is 127 g, and the overall weight is 476 g, which indicates the proposed exoskeleton is lightweight and portable. To improve the grasping performance, the multiobjective genetic algorithm is implemented to optimize contact forces, which is to maximize the sum of the forces exerted on the index finger phalanges by the exoskeleton and to minimize the difference between the contact forces. After optimization, the sum of contact forces is risen by 15%, and the difference between forces is decreased by 53%. Furthermore, the admittance control is applied to make the proposed finger exoskeleton more compliant in the preshaping phase, and the admittance control is also implemented to achieve the fingertip grasping force control in the grasping phase. Finally, experiments have been conducted to verify the range of motion, grasping forces, and feasibility of the proposed index finger exoskeleton. The effectiveness of the control algorithm has also been verified by experiments.**

***Index Terms*—Admittance control, assistance, finger exoskeleton, preshaping, shape-adaptive grasping, underactuation.**

I. Introduction

THE world's population is aging, and almost every country in the world is experiencing an increase in the number and proportion of its elderly population [1]. Due to the weak or impaired motor function of the elderly, especially in the hands, the daily life of the elderly has been greatly affected [2], [3]. However, at present, most elderly people are assisted by their families in the operation of daily necessities, which brings burdens to the elderly's families. Therefore, there is an urgent need for intelligent assistive robots that can improve the quality of activities of daily living (ADL) [4].

Fortunately, some wearable hand-assistive exoskeletons have been designed to assist the elderly with weak or impaired hand motor functions to perform ADL operations. Because the hand-assistive exoskeletons are different from the hand rehabilitation exoskeletons and the hand haptic force-feedback exoskeletons, some special design requirements refer to the discussion given in [5] and [6], which are summarized as follows. First, the hand exoskeleton is a close-coupled human-robot system, and the human-robot kinematic compatibility needs to be considered in the mechanical design. Second, the hand-assistive exoskeleton can assist the user to grasp objects in the same way that the human hand naturally grasps. Grasping objects with generic shapes directly affects the quality of assisting ADL operations, which is considered as one of the most critical needs for the hand-assistive exoskeleton. Third, the hand-assistive exoskeleton should be backdriveable, which ensures that the user can move his/her hand freely. Fourth, the hand-assistive exoskeleton should be portable and lightweight (the weight of the wearable part and overall part), so that the user can use the hand-assistive exoskeleton to assist ADL operations. The suggested maximal wearable part of the hand-assistive exoskeletons is less than 500 g [10]. Furthermore, the self-adaptability to the hand size is also significant.

In literature, based on the transmission types, the hand-assistive exoskeletons are divided into three categories: Tendon-based design, pneumatic-based design, and linkage-based design. Hand-assistive exoskeletons with tendon-driven mechanisms have some advantages, such as lightweight and compact [7]–[10]. However, friction between the cable and the conduit makes the system nonlinear and accounts for major losses in tension transmission across the cable. Although the hysteresis characteristic in the system of the tendon-driven exoskeleton can also dampen unwanted involuntary movements, the hysteresis brings challenges to the accurate control of the tendon-driven system.

Hand-assistive exoskeletons with pneumatic-driven mechanisms are normally more compliant, lightweight, and

Manuscript received 19 May 2021; revised 20 August 2021; accepted 25 September 2021. Date of publication 12 November 2021; date of current version 17 October 2022. Recommended by Technical Editor Z. Bi and Senior Editor W.J.C. Zhang. This work was supported in part by the National Natural Science Foundation of China under Grant 62025307 and Grant U1913209, and in part by Beijing Municipal Natural Science Foundation under Grant JQ19020. *(Corresponding author: Long Cheng)*

Houcheng Li, Long Cheng, Ning Sun, and Ran Cao are with the State Key laboratory of Management and Control for Complex Systems, Institute of Automation, Chinese Academy of Sciences, Beijing 100190, China, and also with the School of Artificial Intelligence, University of Chinese Academy of Sciences, Beijing 100049, China (e-mail: lihoucheng2017@ia.ac.cn; long.cheng.1982@gmail.com; sunning2018@ia.ac.cn; caoran2018@ia.ac.cn).

Color versions of one or more figures in this article are available at https://doi.org/10.1109/TMECH.2021.3120030.

Digital Object Identifier 10.1109/TMECH.2021.3120030

comfortable, because of the low elastic modulus of the soft material [11]–[14]. Based on the cavity structure design, the soft pneumatic actuators can exert well-directed forces on the phalanges. However, the overall pneumatic system is usually bulk and heavy, which prevents the system being portable. Moreover, because of the hysteresis and elastic properties of soft materials, the accurate control of the pneumatic-driven hand-assistive exoskeletons is a challenging task too.

State-of-the-art hand-assistive exoskeletons mostly adopt rigid link structures [15]–[20] for maintenance and reliability comparing to tendon-based and pneumatic-based designs. Rigid link structures possess higher force transmission efficiency and generate more stable force transmissions. The bidirectional movement (flexion and extension) can easily be realized by linkage-based designs. Furthermore, precise dynamic models of the linkage-based hand-assistive exoskeletons are easier to establish than tendon-based and pneumatic-based hand-assistive exoskeletons. To reduce the exoskeleton's overall weight and improve the exoskeleton's portability, underactuation is a good candidate for the linkage-based hand-assistive exoskeletons compared to the full actuation. Underactuation has been widely used in the dexterous robotic hands/grippers design, and many linkage-based underactuated robotic hands/grippers have been designed to complete grasping and operation tasks in industrial scenarios [21]–[26]. As a close-coupled human-robot system, the wearable underactuated hand exoskeletons is different from the underactuated robotic hands/grippers, which should consider the human-robot kinematic compatibility in the mechanical design. In [18], a linkage-based underactuated finger exoskeleton is designed to help the patients do grasping tasks. This exoskeleton is placed on the lateral side of the finger to realize the remote center of motion capability. Although this exoskeleton structure is more compact, this mechanical design cannot always ensure the human-robot axes alignment. Moreover, this hand exoskeleton cannot realize finger preshaping for grasping and lacks backdriveability. In [17], a linkage-based underactuated finger exoskeleton considering the human-robot kinematic compatibility is designed for elderly people to perform grasping tasks. Although it achieves the shape-adaptive grasp for different objects, it lacks the backdriveability and the finger preshaping for grasping. Moreover, its mechanism is not compact and may affect the movement of the wrist. In [15], the authors have proposed a linkage-based underactuated finger exoskeleton for the treatment of tendon injuries. However, it does not consider human-robot kinematic compatibility. Finger preshaping and backdriveability are also absent in this design.

Although underactuated robotic hands can grasp an object with fewer actuators, the contact forces on different phalanges cannot be independently controlled. Underactuated mechanism control algorithms focusing on grasping are mainly based on PID control and impedance control [27]. The PID control is implemented for position control, and the impedance control indirectly adjusts the contact force through a mechanical impedance. In [28], one of the first underactuated robotic hands is designed. Their control problem needs to define the posture of the target hand configuration according to the object to be grasped, and then they use the PD controller to guide the hand to this posture. In [29], sliding-mode impedance control is proposed for an underactuated robotic gripper, which requires the dynamics of the mechanism, and it is difficult to extend to exoskeletons due to the uncertainty of the human model. In [17], the authors propose a rendering strategy based on the impedance control for the underactuated hand exoskeleton. The proposed strategy aims to minimize the error between the desired and the actual output force or pose in the force and operational spaces, respectively.

By the above observations, the purpose of this study is to develop a novel linkage-based underactuated finger exoskeleton to assist grasping for the elderly with weak muscle strength. In the mechanism design of the proposed exoskeleton, the human finger is considered as part of the mechanism to build a virtual four-bar mechanism, which realizes the self-aligning capability of the exoskeletons joint with the corresponding joint of the human finger. Meanwhile, this design can achieve an adaptable kinematic design for different hand sizes without any mechanical adjustment. The movements of the proposed exoskeleton contain two phases: Preshaping phase and grasping phase. Before contact occurs on the phalange, the movements of the metacarpophalangeal (MCP), the proximal interphalangeal (PIP), and the distal interphalangeal (DIP) joints are coupled together, which is called the preshaping phase. After contact occurs on the phalange, the proposed finger exoskeleton can grasp objects with generic shapes. To avoid the ejection phenomenon and achieve the stable grasp, a multiobjective genetic algorithm (MOGA) is implemented to optimize the contact forces. Moreover, the admittance control algorithm is implemented to obtain a compliant behavior in the preshaping phase (called actively backdriveable) and is also adopted to realize fingertip force control for stabilizing grasp strength in the grasping phase. Finally, the experiments are conducted to verify the feasibility of the proposed exoskeleton and to validate the performance of the control algorithm.

The contributions of this article are summarized as follows:

1) From the mechanical design point of view, compared to other linkage-based underactuated hand exoskeletons, to the best of the authors' knowledge, the proposed index finger exoskeleton with the human-robot kinematic compatibility is the first one to achieve the finger preshaping and shape-adaptive grasp of objects with different sizes and shapes.
2) From the portability and transparency point of view, the proposed exoskeleton is more portable and lightweight (wearable part: 127 g, and overall weight: 476 g), so that the user can use the hand exoskeleton to assist ADL operations. Moreover, the proposed exoskeleton is highly transparent because it is actively and passively backdriveable.

The rest of this article is organized as follows. The mechanical design and optimization of the proposed finger exoskeleton is described in Section II. In Section III, the admittance control algorithm is presented. Section IV gives experiments to validate the feasibility of the proposed finger exoskeleton, and experiments are also conducted to verify the control performance. Finally, Section V concludes this article.

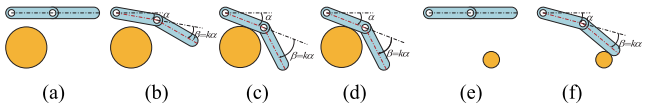

Fig. 1. Grasping process of two-joint finger with coupled mechanism. The coupled coefficient of rotation angle between the two joints is k. (a)–(d) Present the power grasping process. (e)–(f) Present the precision grasping process.

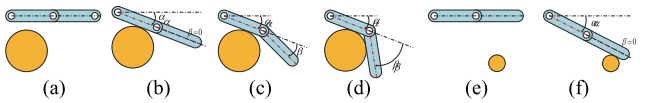

Fig. 2. Grasping process of two-joint finger with self-adaptive mechanism. The two joints rotate separately, and grasp the object with generic shapes.

II. Mechanical Design

A. Motivation

Human grasping motion can be divided into reaching, preshaping, and grasping phases [27]. Much of literature refers to two grasps defined by Napier who suggests a scheme in which grasps are divided into power grasps and precision grasps [30]. Compared to the 21 degree of freedom (DoFs) kinematic model of the human hand, Cobos's work is focused on obtaining an efficient human hand model by simplifying the hand model with 9 DoFs, which has been proved to be more suitable for manipulation tasks by hand robots [31]. One of the simplifications is to add intrafinger constraints. Regarding power grasps, the intrafinger constraints are $\theta_{\mathrm{MCPf/e}} = \frac{4}{3}\theta_{\mathrm{PIP}}$ and $\theta_{\mathrm{PIP}} = \frac{3}{2}\theta_{\mathrm{DIP}}$, where $\theta_{\mathrm{MCPf/e}}, \theta_{\mathrm{PIP}}$, and θ_{DIP} are the flexion/extension joint angles of the MCP, PIP, and DIP joints, respectively. Regarding precision grasps, the intrafinger constraints are $\theta_{\mathrm{MCPf/e}} = \frac{3}{2}\theta_{\mathrm{PIP}}$ and $\theta_{\mathrm{PIP}} = 2\theta_{\mathrm{DIP}}$. The above intrafinger constraints reduce the complexity of hand robot design when retaining the maximum grasping efficiency of natural human hands, which provides a basis for the design of the hand exoskeleton in the preshaping phase.

In traditional single-motor-driven finger exoskeletons, there are two types of designs: Coupled design and self-adaptive design. As shown in Fig. 1, the coupled mechanical design is beneficial to the precision grasp which is consistent with the preshaping movement of the finger. However, in the power grasping process, when the first phalange touches the object, the second phalange may not touch the object shown in Fig. 1, which means the coupled hand exoskeletons cannot realize self-adaptive grasp of objects with different sizes and shapes. Therefore, the mechanical design of only coupling joints together is not suitable for assistive hand exoskeletons. To this end, the self-adaptive design of the assistive hand exoskeleton is proposed. The self-adaptive exoskeleton can achieve the adaptive grasp of objects with different sizes and shapes, whose characteristic is more conducive to power grasp. However, the self-adaptive exoskeleton is not favorable at precision grasp, because the second joint cannot rotate before the first phalange contacts the object as presented in Fig. 2, which is not consistent with the preshaping of the human finger. Therefore, considering the preshaping and the self-adaptive grasping, the coupled and self-adaptive mechanical design is proposed to design an assistive finger exoskeleton that is more in line with the natural movement of human hands as demonstrated in Fig. 3.

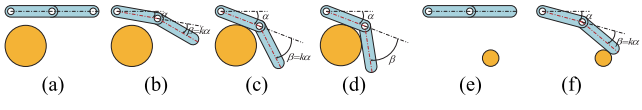

Fig. 3. Grasping process of two-joint finger with coupled and self-adaptive mechanism. Before touching object, the two joins are coupled together, and the coupled coefficient is k. After first phalange touching object, the second join can adapt to the shape of the object.

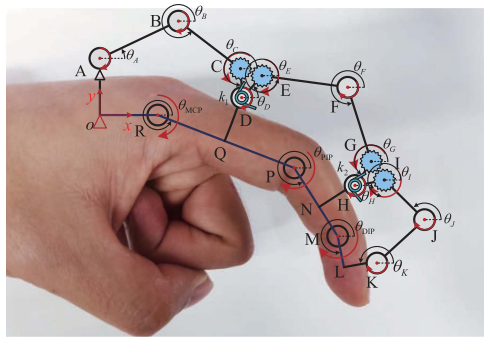

Fig. 4. Kinematic model parameters of the proposed index finger exoskeleton.

B. Kinematics Analysis

The definition of kinematic parameters of the proposed finger exoskeleton is shown in Fig. 4. The kinematics of the finger exoskeleton contains two phases: Preshaping phase and grasping phase, which is divided by whether or not phalanges touch the object. In power-grasp tasks, the proposed exoskeleton actuates the MCP, PIP, and DIP joints of the human finger together until the proximal phalange first reaches and touches the grasping object. When the motion of the MCP joint is constrained due to the contact forces on the proximal phalange, the PIP and DIP joints continue flexing until the intermediate phalange reaches and touches the grasping object. When the motion of the PIP joint is constrained due to the contact forces on the intermediate phalange, the DIP joint also continues flexing until the distal phalange reaches and touches the grasping object. Similarly, the extension of the finger starts from the DIP joint and then is transmitted to the PIP joint, finally is transmitted to the MCP joint until the finger is totally extended and the finger joints reach their physical limits. In precision-grasp tasks, the proposed exoskeleton moves the MCP, PIP, and DIP joints of the human finger simultaneously until the distal phalange reaches and touches the grasping object, rather than moves the MCP, PIP, and DIP joints of the human finger successively. The preshaping phase is beneficial to precise hand operations, closely similar to the human finger movement, and improve the grasping efficiency of the assistive hand exoskeleton compared to the cases without finger preshaping.

In the kinematic model, the coordinate frame is located at the point o which is related to the position of the motor and the MCP joint. The MCP, PIP, and DIP joints of the human finger are defined as points R, P and M, respectively, with

the rotations specified as θ_{MCP}, θ_{PIP}, and θ_{DIP}. A dc motor is attached to point A with the corresponding rotation θ_A, and link oA is grounded. Linkages oR, RP, PM, and ML represent the metacarpal, the proximal phalange, the middle phalange, and the distal phalange, respectively. The mechanism consists of 10 passive revolute joints at points B, C, D, E, F, G, H, I, J and K while their rotations are represented as θ_i for point i. θ_{ij0} represents the initial angle between the point i and point j when the finger is in full extension. l_{ij} represents the length between the point i and point j. In particular, the revolute joints C and E are meshed together by gear structure, which the same design applies to the revolute joints G and I. Through changing the gear ratio among revolute joints C, E and G, I, the coupled rotations of the MCP, PIP and DIP joints would be changed. In this article, the gear ratio between revolute joints C, E is 1:1, and the gear ratio between revolute joints G, I is 0.7:1. The coupled relationships among the MCP, PIP and DIP joints referring to the above-mentioned intrafinger constraints are $\theta_{\mathrm{MCPf/e}} = \frac{4}{3}\theta_{\mathrm{PIP}}$ and $\theta_{\mathrm{PIP}} = \frac{3}{2}\theta_{\mathrm{DIP}}$. The first torsional spring k_1 constrains the movement of D joint, and the second one k_2 is involved in the H joint movement. The stiffness of two torsional springs is $k_1 = k_2 = 1.17Nmm/deg$ based on the literature [18].

In the preshaping phase, the movements of DIP, PIP, and MCP are coupled together. Because of the preloads of the torsion springs k_1 and k_2, the revolute joints D and H are constrained to keep still. In the grasping phase, the synthesized linkage can mimic the grasping motion of the human middle and distal phalanges, which could realize grasping objects with generic shapes. With the proximal and intermediate phalange touching the grasping object, the revolute joints D and H would, respectively, overcome the preloads of the torsion springs k_1 and k_2 to rotate.

The kinematic model of the proposed exoskeleton consists of three closed-loop chains. The MCP chain of the proposed finger exoskeleton is made up of points A, B, C, D, and R, which consists of a virtual five-bar mechanism. The closed-loop equation of the MCP chain is given by

$$l_{\mathrm{AB}}e^{i\theta_{\mathrm{A}}} + l_{\mathrm{BC}}e^{i\theta_{\mathrm{B}}} + l_{\mathrm{CD}}e^{i\theta_{\mathrm{C}}} = l_{\mathrm{AR}}e^{i\theta_{\mathrm{AR}}} + l_{\mathrm{RD}}e^{i\theta_{\mathrm{RD}}} \quad (1)$$

where l_{AR}, l_{RD} are norms of vectors $\overrightarrow{AR}$ and $\overrightarrow{RD}$, respectively. θ_{AR}, θ_{RD} are the vector angles of $\overrightarrow{AR}$ and $\overrightarrow{RD}$, respectively. θ_{A} and θ_{C} are measured by the hall sensors, and $\theta_{\mathrm{RD}} = \theta_{\mathrm{RD0}} + \theta_{\mathrm{MCP}}$.

The PIP chain of the proposed finger exoskeleton consists of points D, E, F, G, H, and P, which makes up a virtual six-bar mechanism. The closed-loop equation of the proximal chain is given by

$$\begin{aligned} l_{\mathrm{DE}}e^{i\theta_{\mathrm{D}}} + l_{\mathrm{EF}}e^{i\theta_{\mathrm{E}}} + l_{\mathrm{FG}}e^{i\theta_{\mathrm{F}}} + l_{\mathrm{GH}}e^{i\theta_{\mathrm{G}}} \\ = l_{\mathrm{DP}}e^{i\theta_{\mathrm{DP}}} + l_{\mathrm{PH}}e^{i\theta_{\mathrm{PH}}} \end{aligned} \quad (2)$$

where l_{DP}, l_{PH} are norms of vectors $\overrightarrow{DP}$ and $\overrightarrow{PH}$, respectively. θ_{DP}, θ_{PH} are the vector angles of $\overrightarrow{DP}$ and $\overrightarrow{PH}$, respectively. θ_{G} is measured by the hall sensor, $\theta_{\mathrm{D}} = \theta_{\mathrm{C}} - \pi - \theta_{\mathrm{DC0}} - \theta_{\mathrm{D0}}$, $\theta_{\mathrm{DP}} = \theta_{\mathrm{DP0}} + \theta_{\mathrm{MCP}}$, and $\theta_{\mathrm{PH}} = \theta_{\mathrm{PH0}} + \theta_{\mathrm{PIP}}$.

The DIP chain of the proposed finger exoskeleton is composed of points H, I, J, K, and M, which consists of a virtual five-bar mechanism. The closed-loop equation of the distal chain is given by

$$l_{\mathrm{HI}}e^{i\theta_{\mathrm{H}}} + l_{\mathrm{IJ}}e^{i\theta_{\mathrm{I}}} + l_{\mathrm{JK}}e^{i\theta_{\mathrm{J}}} = l_{\mathrm{HM}}e^{i\theta_{\mathrm{HM}}} + l_{\mathrm{MK}}e^{i\theta_{\mathrm{MK}}} \quad (3)$$

where l_{HM}, l_{MK} are norms of vectors $\overrightarrow{HM}$ and $\overrightarrow{MK}$, respectively. θ_{HM}, θ_{MK} are the vector angles of $\overrightarrow{HM}$ and $\overrightarrow{MK}$, respectively. $\theta_{\mathrm{H}} = \theta_{\mathrm{G}} - \pi - \theta_{\mathrm{HG0}} - \theta_{\mathrm{H0}}$, $\theta_{\mathrm{HM}} = \theta_{\mathrm{HM0}} + \theta_{\mathrm{PIP}}$, and $\theta_{\mathrm{MK}} = \theta_{\mathrm{MK0}} + \theta_{\mathrm{DIP}}$.

In the 10 passive joints at points B, C, D, E, F, G, H, I, J, and K, $\{\theta_{\mathrm{B}}, \theta_{\mathrm{D}}, \theta_{\mathrm{F}}, \theta_{\mathrm{H}}, \theta_{\mathrm{J}}\}$ are independent variables, and $\{\theta_{\mathrm{C}}, \theta_{\mathrm{E}}, \theta_{\mathrm{G}}, \theta_{\mathrm{I}}, \theta_{\mathrm{K}}\}$ are not independent variables. Therefore, there are six unknown variables $\{\theta_{\mathrm{B}}, \theta_{\mathrm{F}}, \theta_{\mathrm{J}}, \theta_{\mathrm{MCP}}, \theta_{\mathrm{PIP}}, \theta_{\mathrm{DIP}}\}$, and there are three known variables $\{\theta_{\mathrm{A}}, \theta_{\mathrm{C}}, \theta_{\mathrm{G}}\}$ which are measured by hall sensors. Through solving the above nonlinear kinematics equations by using the Levenberg–Marquardt algorithm, the numerical solutions of $\mathbf{X} = [\theta_{\mathrm{MCP}}, \theta_{\mathrm{PIP}}, \theta_{\mathrm{DIP}}]$ can be obtained by given $\mathbf{\Theta_a} = [\theta_{\mathrm{A}}, \theta_{\mathrm{D}}, \theta_{\mathrm{H}}]$.

The velocity kinematics can be obtained by differentiating the position kinematics equations of the MCP, the PIP, and the DIP chains as follows:

$$\dot{\mathbf{X}} = \mathbf{J_A}(\mathbf{\Theta_a})\dot{\mathbf{\Theta}}_\mathbf{a} \quad (4)$$

where $\dot{\mathbf{X}}$ is the velocity vector of the human joints, $\mathbf{J_A}(\mathbf{\Theta_a})$ is the Jacobian matrix, $\dot{\mathbf{\Theta}}_\mathbf{a}$ is the input velocity vector of the exoskeleton joints including motor velocity and two torsional spring velocity.

Remark 1: In the mechanical design, the user's finger phalanges are considered as a part of the kinematic chain to consist of virtual closure-loop chains, which achieves the human-robot kinematic compatibility and realizes self-adaptability to hand size. Meanwhile, it is obvious that the proposed finger exoskeleton can not only achieve enveloping grasp of objects with different shapes and sizes but also efficiently realize the finger preshaping for grasping.

C. Kinetostatic Analysis

The kinetostatic analysis is to ensure the stability of the grasping forces, which has been already introduced previously for a generic underactuated finger with n DOFs [32]. Based on the virtual power principle, the input and the output virtual powers could be calculated as follows:

$$\mathbf{\Psi^T}\dot{\mathbf{\Theta}}_\mathbf{a} = \mathbf{f^T v} \quad (5)$$

where $\mathbf{\Psi} = [\tau_a, -k_1\theta_{\mathrm{D}}, -k_2\theta_{\mathrm{H}}]^T$ is the input torque vector including the torque of the motor and the springs. $\dot{\mathbf{\Theta}}_\mathbf{a} = [\dot{\theta}_{\mathrm{A}}, \dot{\theta}_{\mathrm{D}}, \dot{\theta}_{\mathrm{H}}]^T$ is the vector of the corresonding angular velocity. $\mathbf{f} = [f_1, f_2, f_3]^T$ is the vector of contact wrenches which is simplified as the vector of the normal contact forces. f_1, f_2, and f_3 are the magnitude of normal contact force acting at the proximal phalange, intermediate phalange, and distal phalange, respectively. $\mathbf{v}$ is the vector of the corresponding contact twist.

The contact twist can be simply expressed as the product of a Jacobian matrix and the derivatives of the phalanx joint

coordinates, i.e., $\mathbf{v} = \mathbf{J_C}\dot{\mathbf{X}}$, where $\mathbf{J_C}$ is the contact matrix which is related to the position of contact points.

Therefore, the contact forces f could be calculated as follows:

$$\mathbf{f} = \mathbf{J_C^{-T}}\mathbf{J_A^{-T}}\mathbf{\Psi} \tag{6}$$

where

$$\mathbf{J_C} = \begin{bmatrix} x_1 & 0 & 0 \\ x_2 + l_{\mathrm{RP}}c(\theta_2) & x_2 & 0 \\ x_3 + l_{\mathrm{RP}}c(\theta_2+\theta_3) + l_{\mathrm{PM}}c(\theta_3) & x_3 + l_{\mathrm{PM}}c(\theta_3) & x_3 \end{bmatrix}$$

where x_1, x_2, x_3 are the distances from contact points to R, P, and M, respectively. c and s represent cos and sin, respectively.

D. Optimization of Contact Forces

To properly design underactuated fingers, one should be aware of the ejection phenomenon, which means the finger slides and pushes the object out instead of a secure grasping due to the negative contact force. To avoid the ejection phenomenon and achieve the stable grasp, the exerted contact forces by three phalanges to the object should be positive and distributed as evenly as possible [32], which is referred to as the "force isotropy." Moreover, one should avoid the possibility that the last phalange force is too small to ensure the stable grasping. Therefore, in the optimization, considering the ejection phenomenon and the stable grasping, one of the optimization objectives is to minimize the difference between the three contact forces, and another optimization objective is to maximize the sum of the forces exerted on the index finger phalanges by the proposed finger exoskeleton, which are expressed as follows:

$$\begin{aligned} &\text{Objective 1}: \max F(X) = \sqrt{f_1^2 + f_2^2 + f_3^2} \\ &\text{Objective 2}: \min F_{\mathrm{dif}}(X) = \max(f_1, f_2, f_3) - \min(f_1, f_2, f_3). \end{aligned} \tag{7}$$

In the optimization, the posture of the finger is determined by the MCP, PIP, and DIP joint angles of the index finger. The desired values of joint angles are $20°, 50°, 30°$ because the resulting finger's posture is suitable for the spherical and cylindrical grasping, which are two most commonly used operations in daily operations [33]. There are ten linear constraints $X = [l_{\mathrm{AB}}, l_{\mathrm{BC}}, l_{\mathrm{CD}}, l_{\mathrm{DE}}, l_{\mathrm{EF}}, l_{\mathrm{FG}}, l_{\mathrm{GH}}, l_{\mathrm{HI}}, l_{\mathrm{IJ}}, l_{\mathrm{JK}}]$. The initial values for the lengths have been determined by the experiment based on a CAD software by motion analysis. The initial values can guarantee feasible motion of the exoskeleton. However, it cannot guarantee the optimal motion. In the optimization search space, the lower bound of the lengths of the linkages is assumed to be $0.5\times$ (initial lengths), and the upper bound is assumed to be $1.5\times$ (initial lengths). These limits have been chosen in order to look for solutions in a reasonably wide search space to avoid too many nonmechanically feasible kinematics. The nonlinear constraints are expressed as follows:

$$\begin{cases} 80° \le \theta_{\mathrm{MCP}}(X), \theta_{\mathrm{PIP}}(X), \theta_{\mathrm{DIP}}(X) \le 90° \\ \theta_{\mathrm{tranMCP}}(X), \theta_{\mathrm{tranPIP}}(X), \theta_{\mathrm{tranDIP}}(X) \ge 50° \end{cases} \tag{8}$$

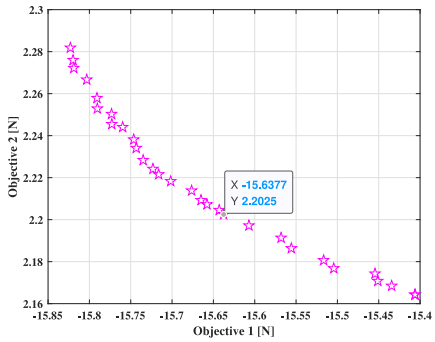

Fig. 5. Pareto front of the multiobjective optimization result.

TABLE I
INITIAL LENGTHS OF THE LINKAGES, THE LOWER BOUND AND UPPER BOUND OF SEARCH SPACE, AND THE OPTIMIZED LENGTHS

Linkage [mm]	Initial lengths	Lower bound	Upper bound	Optimized length
l_{AB}	30	15	45	31.74
l_{BC}	25	12.5	37.5	37.21
l_{CD}	6	3	9	7.96
l_{DE}	6	3	9	8.23
l_{EF}	30	15	45	39.88
l_{FG}	25	12.5	37.5	36.99
l_{GH}	6	3	9	8.14
l_{HI}	6	3	9	7.78
l_{IJ}	20	10	30	23.32
l_{JK}	20	10	30	27.97

where $\theta_{\mathrm{MCP}}(X)$, $\theta_{\mathrm{PIP}}(X)$, and $\theta_{\mathrm{DIP}}(X)$ represent the MCP, PIP, and DIP joint angles, respectively. $\theta_{\mathrm{tranMCP}}(X)$, $\theta_{\mathrm{tranPIP}}(X)$, $\theta_{\mathrm{tranDIP}}(X)$ are corresponding mechanism transmission angles.

As previously mentioned, the optimization has been performed by a MOGA called NSGA-II proposed by Deb *et al* [34]. The designed genetic algorithm works with a population of 100 individuals. Moreover, the stall generation limit is set to 500. In details, the algorithm is programmed to stop when the cumulative change in the fitness function value over 10 generations is less than 10^{-8}.

After optimization, the Pareto front of the multiobjective optimization result is shown in Fig. 5, and the solution corresponding to coordinate point (-15.64, 2.20) is chosen as the Pareto optimal solution. In Table I, it is possible to notice that none of the optimized lengths is on the boundary of the search space, which means the lower and upper bound of search space are set reasonably. In Table II, the ranges of motions of the MCP, PIP, and DIP joint angles are significantly improved, and they are between 80 degrees and 90 degrees. Meanwhile, the corresponding mechanism transmission angles are also greater than 50°, which ensures better transmission efficiency of the mechanism. In Table III, after the optimization, the contact force f_1 goes down a little bit, and the contact forces f_2, f_3 go up significantly. During the optimization, the Objective 1 is risen by 15%, and the Objective 2 is decreased by 53%.

TABLE II
INITIAL ANGLES AND OPTIMIZED ANGLES OF THE MCP, PIP, AND DIP JOINT ANGLE AND THE CORRESPONDING MECHANISM TRANSMISSION ANGLES

Angle	Initial angle [°]	Optimized angle [°]
$\theta_{\mathrm{MCP}}(X)$	44.19	87.37
$\theta_{\mathrm{PIP}}(X)$	57.61	84.16
$\theta_{\mathrm{DIP}}(X)$	61.04	82.08
$\theta_{\mathrm{tranMCP}}(X)$	56.20	68.25
$\theta_{\mathrm{tranPIP}}(X)$	62.21	69.29
$\theta_{\mathrm{tranDIP}}(X)$	47.51	51.31

TABLE III
INITIAL FORCES AND OPTIMIZED FORCES OF THE MCP, PIP, AND DIP JOINT

Contact force	f_1	f_2	f_3	Obj. 1	Obj. 2
Initial force [N]	10.54	5.39	6.47	13.49	5.15
Optimized force [N]	10.26	8.06	8.63	15.64	2.20

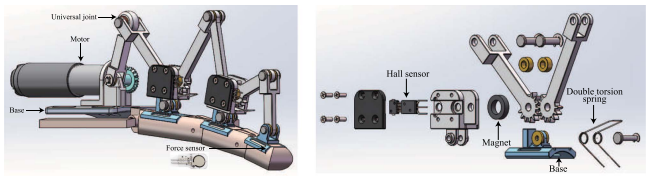

(a) (b)

Fig. 6. CAD model of the proposed finger exoskeleton: (a) Overall view of the proposed finger exoskeleton. (b) Exploded view of the proximal phalange part of the proposed finger exoskeleton.

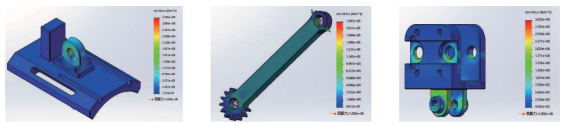

(a) (b) (c)

Fig. 7. Finite element analysis for different linkages strength.

Remark 2: Through the multiobjective optimization, the total grasping forces are improved, and the difference of grasping forces between the individual phalanx is significantly reduced. Meanwhile, the ranges of motions of the MCP, PIP, and DIP joint angles are improved compared to the case before optimization, and can meet the needs of users. The optimization results are validated in the experiment, which is presented in Section IV-A.

E. Prototype Design

Based on the above optimization, the optimized lengths of all linkages are obtained to guide the manufacture of the proposed exoskeleton. The prototype of the proposed finger exoskeleton is designed whose CAD model is shown in Fig. 6(a). The finite element analysis for the proposed exoskeleton is conducted for analyzing the mechanical design. In the simulation, apply 20-N force to the contact surface of the linkages, and then calculate the stress of the linkages under this load. As shown in Fig. 7, the maximum stress generated by each linkage is less than the yield strength of the aluminium alloy material, which means there is no weak linkage in the proposed finger exoskeleton. All linkages of the proposed finger exoskeleton are made of aluminium to reduce the system weight, and all bases of the proposed finger exoskeleton are made of resin material by 3D printing. The proposed finger exoskeleton is actuated by a dc motor (1741U012CXR123, FAULHABER, Germany) with a reduction box (50:1, FAULHABER, Germany) that is mounted on the back of the palm and can be easily worn by buckling the Velcro straps. Because of the low gear reduction ratio, the proposed finger exoskeleton is easy to achieve passive backdriveability. The passive backdriveability force is 1.2 N measured by a force sensor as shown in Fig. 6(a), which means the users can easily move their fingers freely while wearing the proposed finger exoskeleton. In order not to restrict the adduction–abduction movement of the MCP joint, a universal joint is implemented as a passive DOF in the MCP chain as shown in Fig. 6(a). Hall sensors with magnets mounted at the joints are used to measure the joints' angles presented in Fig. 6(b), and the dc motor encoder is also used to indirectly measure the joints' angles. The double torsion springs shown in Fig. 6(b) are preloaded and mounted at the joints, which are compressed during the grasping phase to realize the shape adaptation capability. The force sensors (FlexiForce a301, USA) are used to measure the man-robot interaction forces, which is mounted between the distal phalange and the base of the proposed finger exoskeleton as shown in Fig. 6(a). The wearable part of the proposed finger exoskeleton is 127 g (including the dc motor), and the overall weight of the proposed finger exoskeleton is 476 g (including microcontroller, battery, etc.). In [10], it suggests that 10 N of pinch grip force is a reasonable goal for a hand exoskeleton, which is sufficient to lift objects weighing up to 1 kg, for example, to drink from water bottles (750 mL) independently. In the current design, the maximum fingertip force generated by the proposed exoskeleton is about 12.3 N that is measured by a dynamometer. This is sufficient for the power grasping task for lifting objects required in daily activities. Compared to typical linkage-based, tendon-based, and pneumatic-based assistive hand exoskeletons in the literature, the advantages of the proposed finger exoskeleton are listed in Table IV.

As regards to safety, first, there is a mechanical stop on the motor base to prevent overextension and overflexion of finger joints in the current design. The proposed exoskeleton is backdriveable, which ensures that the user can move his/her finger freely without restrictions. Second, the safety is also ensured by the control software. Since the force sensors are used to measure the human-robot interaction force and the hall sensors are used to measure the finger's motion, the real-time force and joint angle information can be transmitted back to the microcontroller. Third, there is an emergency switch in the proposed finger exoskeleton. Once the user feels the interaction force is too large or feels uncomfortable, he/she can stop the exoskeleton immediately.

Remark 3: The proposed finger exoskeleton is lightweight and portable compared to other linkage-based underactuated finger exoskeletons. Moreover, the proposed finger exoskeleton

TABLE IV
CHARACTERISTICS COMPARISONS WITH SOME TYPICAL ASSISTIVE FINGER EXOSKELETONS

Typical exoskeletons	Number of finger	Mechanism	Finger preshaping	Passive backdriveability	Kinematic compatibility	Fingertip force	Wearable weight	Overall weight
Hong [18]	1	linkage				10N	172g	-
Sarac [17]	3	linkage			✓	14.9N	300g	-
Ertas [15]	1	linkage				-	185g	-
Kang [9]	2	tendon			✓	10N	104g	1140g
Bützer [10]	5	tendon			✓	6.4N	148g	868g
Heung [13]	5	pneumatic			✓	-	207g	-
Proposed	1	linkage	✓	✓	✓	12.3N	127g	476g

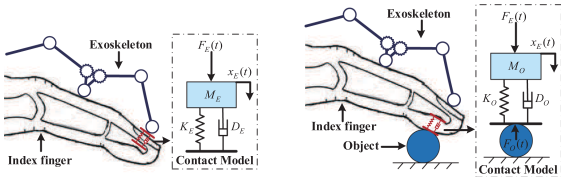

(a) (b)

Fig. 8. (a) Contact model of the proposed finger exoskeleton with the index finger. (b) Contact model of the human-robot system with the object.

is featured by the finger preshaping and the passive backdriveability from the mechanical design, which is not possessed by other exoskeletons.

III. CONTROL ALGORITHM

In order to actively assist hand grasp in ADL by the proposed finger exoskeleton, the admittance control is used to achieve human-robot interaction force control. In the preshaping phase, the control objective is to minimize the interaction force between the proposed finger exoskeleton and the human index finger, which is to make the robot system obtain a compliant behavior by control, also called active backdrivability. In the grasping phase, the control objective is to reduce the fingertip interaction force error between the desired grasping force and the actual grasping force.

A. Admittance Control in the Preshaping Phase

In the preshaping phase, the human-robot system does not contact with the object, and minimizing interaction force between the proposed finger exoskeleton and the index finger is mainly considered. To make the proposed finger exoskeleton more compliant, the admittance control is used. Admittance control is typically utilized to obtain a compliant behavior on industrial robots, since they are characterized by a stiff and nonbackdrivable mechanical structure, which is proposed by Hogan [35]. The contact model of the proposed finger exoskeleton with the index finger is shown in Fig. 8(a). The contact model is formulated as follows:

$$M_E(\ddot{x}_D - \ddot{x}_0) + D_E(\dot{x}_D - \dot{x}_0) + K_E(x_D - x_0) = F_E \quad (9)$$

where x_0 is the initial desired fingertip trajectory in the preshaping phase. x_D is the newly generated desired trajectory under the admittance control. M_E, D_E, and K_E are the desired inertia, damping, and stiffness in the preshaping phase, respectively. F_E is the human-robot interaction force on the distal phalange that is measured by the force sensor.

Because the proposed finger exoskeleton itself has the backdrivability in mechanical structure, the M_E, D_E, and K_E can be identified by its inherent backdrivability. By collecting the contact force and finger joints' angles in the case of the proposed finger exoskeleton without driving, the least square method is implemented to identify the parameters of the contact model.

The (9) can be rewritten as follows:

$$\ddot{x}_D = \ddot{x}_0 + \frac{1}{M_E}\left(F_E - D_E(\dot{x}_D - \dot{x}_0) - K_E(x_D - x_0)\right). \quad (10)$$

The desired acceleration of the proposed finger exoskeleton is acquired by (10). By integrating the desired acceleration, the desired position of the proposed finger exoskeleton can be obtained.

To make the actual trajectory of the proposed finger exoskeleton track the desired ideal trajectory, the PID controller is implemented as follows:

$$u(t) = K_p \cdot e(t) + K_i \cdot \int_0^t e(t)dt \cdot + K_d \cdot \dot{e}(t) \quad (11)$$

where $u(t)$ is the output of the PID controller, $e(t) = x_D(t) - x_E(t)$ is the tracking error, K_p, K_i, and K_d are the proportional, integral, and differential gains of the PID controller, respectively. x_E is the fingertip position of the proposed finger exoskeleton which is measured by the Hall sensor.

Remark 4: The admittance control is implemented to achieve the active backdriveability of the proposed finger exoskeleton, which means the users can move their fingers freely when they wear the proposed finger exoskeleton in the preshaping phase. This is proven in Section IV-C.

B. Admittance Control in the Grasping Phase

In the grasping phase, the human-robot system contacts with the object, and the main concern is to ensure that the fingertip interaction forces meet the expectations. The contact model of the human-robot system with the object is shown in Fig. 8(b). The contact model is formulated as follows:

$$M_O(\ddot{x}_D - \ddot{x}_O) + D_O(\dot{x}_D - \dot{x}_O) + K_O(x_D - x_O) = F_E - F_O \quad (12)$$

TABLE V
ACTIVE AND PASSIVE ROM RESULTS OF TWO SUBJECTS WITHOUT AND WITH THE EXOSKELETON

Subject	joint	Active RoM				Passive RoM	
		Without		With			
		Fl.	Ex.	Fl.	Ex.	Fl.	Ex.
Subj.#1	MCP f/e	86.5°	0.8°	81.1°	1.2°	79.7°	2.1°
	PIP f/e	95.4°	2.5°	82.7°	0.9°	78.9°	1.7°
	DIP f/e	89.7°	1.2°	80.3°	3.4°	76.6°	0.5°
Subj.#2	MCP f/e	89.8°	3.5°	82.5°	0.8°	81.1°	1.5°
	PIP f/e	98.6°	0.8°	85.4°	3.2°	82.7°	0.9°
	DIP f/e	90.1°	1.4°	82.8°	2.1°	78.9°	2.8°

*Fl. and Ex. represents flexion and extension motion, respectively.

where x_O is the initial desired fingertip position in the grasping phase, x_D is the newly generated desired trajectory under the admittance control. M_O, D_O, and K_O are the desired inertia, damping, and stiffness in the grasping phase, respectively. F_E is the actual fingertip interaction force between the human-robot system and the object which is measured by the force sensor, and F_O is the desired fingertip interaction force between the human-robot system and the object. The initial desired position x_O in the grasping phase is confirmed as follows:

$$x_O = x_{O0} + \frac{F_D}{K_O} \tag{13}$$

where the x_{O0} is the position that the fingertip makes contact with the object that the fingertip just contacts the object.

The (12) is rewritten as follows:

$$\ddot{x}_D = \ddot{x}_O + \frac{1}{M_O}\left(F_E - F_O - D_O(\dot{x}_D - \dot{x}_O) - K_O(x_D - x_O)\right). \tag{14}$$

By integrating the ideal acceleration (14), the ideal position of the proposed finger exoskeleton can be obtained in the grasping phase. By the similar procedure (11), the PID control is also implemented to track the desired trajectory.

Remark 5: In the grasping phase, the user wears the proposed finger exoskeleton, and contacts with real objects. The admittance control is adopted to realize constant grasping force control which ensures the grasp stability, which is shown in Section IV-C.

IV. EXPERIMENTAL RESULTS AND DISCUSSIONS

A. Function Verification of the Proposed Finger Exoskeleton

First, two experiments are conducted to test the effect of the exoskeleton on the range of motion (RoM) of the finger by two subjects shown in Table V: Active RoM of the user's own finger without exoskeleton assistance and active RoM of the user's own finger wearing the exoskeleton but without the exoskeleton assistance. Five markers are placed on the index finger's side to obtain the index finger joints' angles measured by motion Ccapture. Table V shows the RoM of finger joints is affected by the mounting placement of the proposed exoskeleton. The results show that the finger joints' active RoM is reduced when the proposed index finger exoskeleton is attached to the subject's hand. Then, the test of the exoskeleton driving the index finger is performed. The exoskeleton is worn on the subject's index finger, assisting the index finger to perform the flexion/extension motions. The passive RoM is shown in right column of the Table V. The affected RoM is slightly smaller than the active RoM. The experimental result of the RoM is consistent with the kinematic analysis in Section II.

TABLE VI
CONTACT FORCES FOR DIFFERENT OBJECTS

Contact force	Cup	Apple	Toothbrush	Pen
f_1	1.87N	2.74N	0.00N	0.00N
f_2	1.73N	2.66N	0.00N	0.00N
f_3	2.01N	2.89N	0.49N	0.26N
Objects' weight	200g	300g	28g	12g

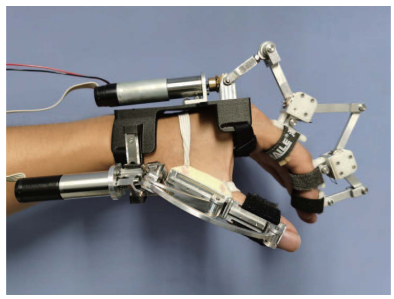

Fig. 9. Prototype of the newly formed hand exoskeleton mounted on the subject's hand.

The experiments are conducted to verify the grasping force. In the experiment, the subject wears the proposed index finger exoskeleton to complete a series of grasping tasks, such as grasping a cup, an apple, a toothbrush, and a pen. Three force sensors are mounted between the proximal phalange, intermediate phalange, distal phalange, and their bases of the proposed exoskeleton, which are used to measure the contact forces. As presented in Table VI, the experimental results show that the differences between three contact forces are small and the measuring contact forces are all positive, which ensures all objects are securely grasped and avoid the ejection phenomenon. This is consistent with the analysis of the contact-force optimization in Section II.

B. Feasibility of the Proposed Finger Exoskeleton

In the experiment, the authors have added a thumb exoskeleton to the proposed index finger exoskeleton to form a complete assistive hand exoskeleton system, which is shown in Fig. 9. The thumb exoskeleton also considers the human-robot kinematic compatibility and grasping adaptability for different objects, which has been proposed in the previous conference paper [36]. The thumb exoskeleton can realize underactuated motions such as thumb flexion/extension, abduction/adduction, and opposition (working with the proposed finger exoskeleton). The weight of the wearable part of the newly formed hand exoskeleton system is 463 g, which is within the suggested maximal weight

Fig. 10. Snapshots on two elderly people's tests by using the proposed hand-assistive exoskeleton.

of assistive hand exoskeletons, which suggests that the maximal wearable part of the hand-assistive exoskeletons is less than 500 g [10]. As to the physical space, the thumb exoskeleton is placed on the back of the hand as shown in Fig. 9. The added exoskeleton does not affect the range of motion of the index finger, and the range of motion of the wrist is also not affected. To validate the feasibility of the hand exoskeleton, the experiments on two elderly subjects (two females, 64 years old, 65 years old) with weak muscle strength have been conducted to complete a series of grasping tasks, such as grasping a cup, an apple, a toothbrush, and a pen, which are shown in Fig. 10. After the assistance process, two elderly people filled out questionnaires about the exoskeleton based on their own usage experiences. In the questionnaire, 10 questions were set up, and the main concern was to get information regarding the usage feedback of the elderly. For example, five levels were roughly set to collect the usage comfortability in the questionnaires: "Very comfortable," "Comfortable," "Neutral," "Uncomfortable," and "Very uncomfortable." Based on the questionnaires, both elderly people chose the "Comfortable" option after assistance. Moreover, two elderly people gave a positive evaluation of the proposed hand exoskeleton. Experimental results also show that two elderly subjects can accomplish different grasping tasks with the help of the proposed hand exoskeleton. Meanwhile, the proposed hand exoskeleton is able to adapt to objects with different shapes and sizes, which is consistent with the mechanical analysis.

C. Effectiveness Verification of the Proposed Control Algorithms

First, the experiment is designed to verify the active backdrivability (compliant ability) of the proposed finger exoskeleton under the admittance control. The values of parameters M_E, D_E, and K_E are identified by the least square method from the proposed finger exoskeleton inherent passive backdrivability in mechanical structure. In the identification experiment, the subjects wore the proposed finger exoskeleton on index finger and completed the movement of their fingers from extension to flexion to extension. Meanwhile, the contact force between the subject's index fingertip and the proposed finger exoskeleton and joint angles were recorded. Based on the least square method, the parameters are obtained M_E=0.05 kg, D_E=11.82 N· s/m, and K_E = 0.12 N/m. In the whole process of identification experiment, the proposed finger exoskeleton is not driven by motor, and it is completely driven by the subject's index finger. In the process of the admittance control, the subject performs two consecutive movements, from extension to flexion and from

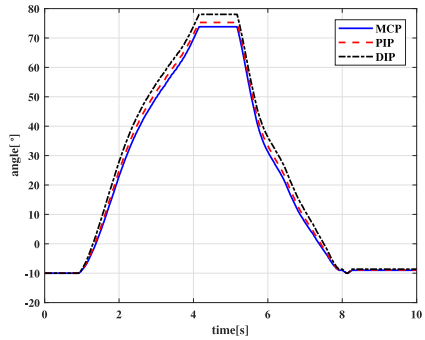

Fig. 11. Curve of the index joints angles under the admittance control.

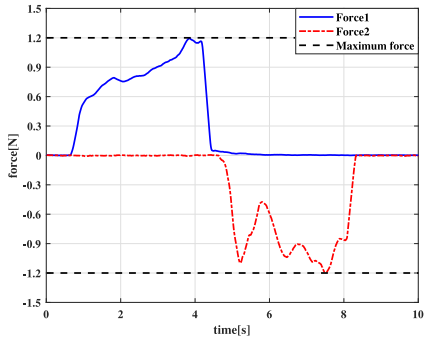

Fig. 12. Curve of the contact forces between the proposed finger exoskeleton with the index finger under the admittance control.

flexion to extension. Fig. 11 shows the curve of the finger joints angles under admittance control. The maximum motion angles of MCP, PIP, and DIP joints are 78.6°, 75.2°, and 73.7°, respectively, which is consistent with the optimized results. Fig. 12 displays the curve of the contact forces between the index finger and the proposed finger exoskeleton under admittance control. The solid line (Force 1) presents the contact force of the finger from extension to flexion, and the dashed line (Force 2) presents the contact force of the finger from flexion to extension. The maximum interaction force is greater than -1.2 N and less than 1.2 N, which means the parameter identification of the M_E, D_E, and K_E is effective. This parameter selection method can minimize the interaction force between the proposed finger exoskeleton and the human index finger compared to trial and error method, and the active backdriveability of the proposed finger exoskeleton can be guaranteed under the admittance control.

Second, the experiment is designed to verify the constant interaction force control of the proposed finger exoskeleton under the admittance control during grasping the object. To obtain the values of parameters M_O, D_O, and K_O, the subject worn the proposed finger exoskeleton on the index finger, and completed the tip pinch (pinching a pen) with the help of the proposed finger exoskeleton. Simultaneously, the contact force between the human-robot system and the object and the joint angles were recorded when the contact force increased from 0 to 1 N. Based on the least square method, the parameters are obtained M_O = 0.05 kg, D_O = 6.74 N· s/m, and K_O = 27.98 N/m. Fig. 13 presents the curve of the contact force between the human-robot system with the object under the admittance control. From the

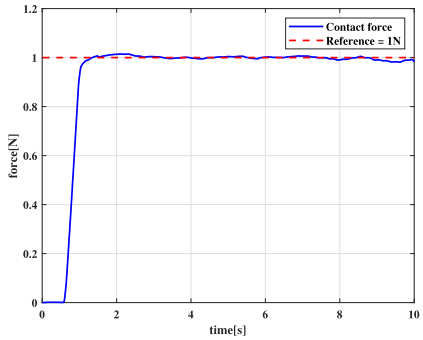

Fig. 13. Contact force between the human-robot system with the object.

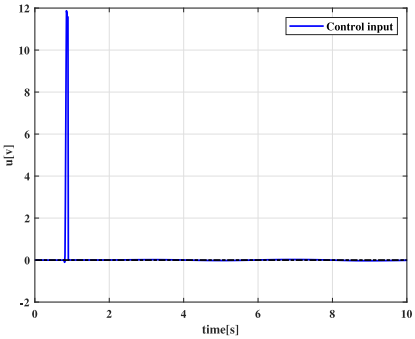

Fig. 14. Curve of the control input under the admittance control.

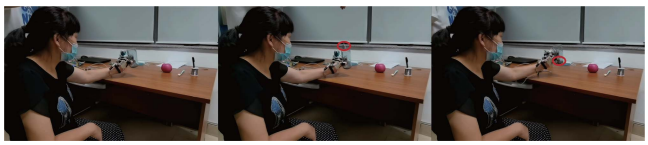

Fig. 15. Adding external disturbances to test the robustness of the admittance controller.

viewpoint of the steady-state error, the maximum steady-state error is 0.1 N. From the transient control performance viewpoint, according to Fig. 13, the settling time of the proposed admittance control is 0.8 s, which indicates the good transient performance of the proposed admittance control for the constant force control. The curve of the contact force control input is presented in Fig. 14.

To further test the robustness of the admittance control system, the authors have considered adding external disturbances. In the test, the elderly subject wears the proposed exoskeleton to grasp a cup. When the user firmly grasps the cup (weight: 100 g) with the assistance of the proposed exoskeleton, the external disturbance is added by adding counterweights (weight: 100 g) in the bottom of the cup shown in Fig. 15. At this point, the control system is affected by external disturbances. The experimental result shows that the exoskeleton can still assist to grasp the cup under the external disturbance, which validates the robustness of the admittance control system.

V. Conclusion

This article proposes a novel underactuated finger exoskeleton to assist the elderly with muscle weakness to grasp objects in activities of daily livings. In the mechanical design, first, the proposed finger exoskeleton achieves the human-robot kinematic compatibility. Second, to realize the finger preshaping, the movement of the MCP, PIP, and DIP are coupled together before the phalanges contact the object. Third, the mechanical structure can adapt to grasp objects with different shapes and sizes. The kinematics and kinetostatics of the proposed finger exoskeleton are analyzed in details. To avoid the ejection phenomenon and achieve the stable grasp, a MOGA is implemented to optimize the contact forces. After optimization, the sum of contact forces is risen by 15%, and the difference between forces is decreased by 53%. Based on the analysis of the contact model between the proposed finger exoskeleton and the human index finger, the admittance control is implemented to realize the active backdrivability of the proposed finger exoskeleton at the control level, and the parameter identification of the admittance control is based on the passive backdrivability characteristics rather than trial and error method. Furthermore, to realize constant contact force control between the human-robot system and the object, the admittance control is also used to achieve the constant force control, and the parameters of the admittance control are also identified from the real object contact process rather than trial and error method. Finally, experiments are implemented to verify the range of motion, grasping force, and feasibility of the proposed finger exoskeleton, and the effectiveness of the proposed control algorithms is also validated in the experiment.

In the future, to better reflect the human-robot interaction impedance, the parameters of the admittance control algorithms are to be updated adaptively rather than constant values. Moreover, more experiments with the elderly need to be conducted for a long period to verify how much assistance the proposed finger exoskeleton can provide.

References

[1] "Revision of the world population prospects," United Nations, Department of Economic and Social Affairs Population Division, New York, NY, USA, ST/ESA/SER.A/423, 2019.

[2] C. Fallaha, M. Saad, J. Ghommam, and Y. Kali, "Sliding mode control with model-based switching functions applied on a 7-DOF exoskeleton arm," *IEEE/ASME Trans. Mechatronics*, vol. 26, no. 1, pp. 539–550, Feb. 2021.

[3] M. R. Haghjoo, H. Lee, M. R. Afzal, A. Eizad, and J. Yoon, "Mech-walker: A novel single-DOF linkage device with movable frame for gait rehabilitation," *IEEE/ASME Trans. Mechatronics*, vol. 26, no. 1, pp. 13–23, Feb. 2021.

[4] D. J. Hyun, H. Lim, S. Park, and S. Nam, "Singular wire-driven series elastic actuation with force control for a waist assistive exoskeleton, H-WEXv2," *IEEE/ASME Trans. Mechatronics*, vol. 25, no. 2, pp. 1026–1035, Apr. 2020.

[5] M. Sarac, M. Solazzi, and A. Frisoli, "Design requirements of generic hand exoskeletons and survey of hand exoskeletons for rehabilitation, assistive, or haptic use," *IEEE Trans. Haptics*, vol. 12, no. 4, pp. 400–413, Oct./Dec. 2019.

[6] Q. A. Boser, M. R. Dawson, J. S. Schofield, G. Dziwenko, and J. S. Hebert, "Defining the design requirements for an assistive powered hand exoskeleton: A pilot explorative interview study and case series," *Prosthetics Orthotics Int.*, vol. 45, no. 2, pp. 161–169, 2021.

[7] D. Popov, I. Gaponov, and J. H. Ryu, "Portable exoskeleton glove with soft structure for hand assistance in activities of daily living," *IEEE/ASME Trans. Mechatronics*, vol. 22, no. 2, pp. 865–875, Apr. 2017.

[8] S. Park, L. Weber, L. Bishop, J. Stein, and M. Ciocarlie, "Design and development of effective transmission mechanisms on a tendon driven hand orthosis for stroke patients," in *Proc. IEEE Int. Conf. Robot. Automat.*, 2018, pp. 2281–2287.

[9] B. B. Kang, H. Choi, H. Lee, and K. J. Cho, "Exo-glove poly II: A polymer-based soft wearable robot for the hand with a tendon-driven actuation system," *Soft Robot.*, vol. 6, no. 2, pp. 214–227, 2019.

[10] T. Bützer, O. Lambercy, J. Arata, and R. Gassert, "Fully wearable actuated soft exoskeleton for grasping assistance in everyday activities," *Soft Robot.*, vol. 8, no. 2, pp. 128–143, 2020.
[11] J. Wang, Y. Fei, and W. Pang, "Design, modeling, and testing of a soft pneumatic glove with segmented PneuNets bending actuators," *IEEE/ASME Trans. Mechatronics*, vol. 24, no. 3, pp. 990–1001, Jun. 2019.
[12] H. Zhang, A. S. Kumar, F. Chen, J. Y. H. Fuh, and M. Y. Wang, "Topology optimized multimaterial soft fingers for applications on grippers, rehabilitation, and artificial hands," *IEEE/ASME Trans. Mechatronics*, vol. 24, no. 1, pp. 120–131, Feb. 2019.
[13] K. H. L. Heung, R. K. Y. Tong, A. T. H. Lau, and Z. Li, "Robotic glove with soft-elastic composite actuators for assisting activities of daily living," *Soft Robot.*, vol. 6, no. 2, pp. 289–304, 2019.
[14] H. Li, L. Cheng, Z. Li, and W. Xue, "Active disturbance rejection control for a fluid-driven hand rehabilitation device," *IEEE/ASME Trans. Mechatronics*, vol. 26, no. 2, pp. 841–853, Apr. 2021.
[15] I. H. Ertas, E. Hocaoglu, D. E. Barkana, and V. Patoglu, "Finger exoskeleton for treatment of tendon injuries," in *Proc. IEEE 11th Int. Conf. Rehabil. Robot.*,, 2009, pp. 194–201.
[16] M. Cempini, M. Cortese, and N. Vitiello,"A powered finger-thumb wearable hand exoskeleton with self-aligning joint axes," *IEEE/ASME Trans. Mechatronics*, vol. 20, no. 2, pp. 705–716, Apr. 2015.
[17] M. Sarac, M. Solazzi, M. A. Otaduy, and A. Frisoli, "Rendering strategies for underactuated hand exoskeletons," *IEEE Robot. Automat. Lett.*, vol. 3, no. 3, pp. 2087–2092, Jul. 2018.
[18] M. B. Hong, S. J. Kim, Y. S. Ihn, G. C. Jeong, and K. Kim, "KULEX-Hand: An underactuated wearable hand for grasping power assistance," *IEEE Trans. Robot.*, vol. 35, no. 2, pp. 420–432, Apr. 2019.
[19] S. W. Pu, Y. C. Pei, and J. Y. Chang, "Decoupling finger joint motion in an exoskeletal hand: A design for robot-assisted rehabilitation," *IEEE Trans. Ind. Electron.*, vol. 67, no. 1, pp. 686–697, Jan. 2020.
[20] S. Ueki *et al.*, "Development of a hand-assist robot with multi-degrees-of-freedom for rehabilitation therapy," *IEEE/ASME Trans. Mechatronics*, vol. 17, no. 1, pp. 136–146, Feb. 2012.
[21] K. Hang, W. G. Bircher, A. S. Morgan, and A. M. Dollar, "Manipulation for self-identification, and self-identification for better manipulation," *Sci. Robot.*, vol. 6, 2021, Art. no. eabe1321.
[22] J. M. Boisclair, T. Laliberte, and C. Gosselin, "On the optimal design of underactuated fingers using rolling contact joints," *IEEE Robot. Automat. Lett.*, vol. 6, no. 3, pp. 4656–4663, Jul. 2021.
[23] X. Shan and L. Birglen, "Modeling and analysis of soft robotic fingers using the fin ray effect," *Int. J. Robot. Res.*, vol. 39, no. 14, pp. 1686–1705, 2020.
[24] F. Wang, Z. Qian, Z. Yan, C. Yuan, and W. Zhang, "A novel resilient robot: Kinematic analysis and experimentation," *IEEE Access*, vol. 8, pp. 2885–2892, 2020.
[25] T. Zhang, W. Zhang, and G. Madan, "Resilient robots: Concept, review, and future direction," *Robot.*, vol. 6, no. 4, 2017, Art. no. 22.
[26] L. Cao, A. T. Dolovich, A. L. Schwab, J. L. Herder, and W. Zhang, "Toward a unified design approach for both compliant mechanisms and rigid-body mechanisms: Module optimization," *ASME J. Mech. Des.*, vol. 137, no. 12, pp. 122301. 1–122301.10, 2015.
[27] R. Ozawa and K. Tahara, "Grasp and dexterous manipulation of multifingered robotic hands: A review from a control view point," *Adv. Robot.*, vol. 31, no. 19, pp. 1030–1050, 2017.
[28] T. Laliberte, L. Birgleny, and C. M. Gosseliny, "Underactuation in robotic grasping hands," *Mach. Intell. Robotic Control*, vol. 4, no. 3, pp. 1–11, 2002.
[29] H. Luo, X. Duan, and D. Hua, "Sliding mode impedance control of a underactuated prosthetic hand," in *Proc. IEEE Int. Conf. Inf. Automat.*,, 2014, pp. 726–729.
[30] J. R. Napier, "The prehensile movements of the human hand," *J. Bone Joint Surg.*, vol. 38B, no. 4, pp. 902–913, 1956.
[31] S. Cobos, M. Ferre, M. A. Sanchéz Urán, J. Ortego, and C. Peña, "Efficient human hand kinematics for manipulation tasks," in *Proc. IEEE/RSJ Int. Conf. Intell. Robots Syst.*, 2008, pp. 2246–2251.
[32] L. Birglen and C. M. Gosselin, "Kinetostatic analysis of underactuated fingers," *IEEE Trans. Robot. Automat.*, vol. 20, no. 2, pp. 211–221, Apr. 2004.
[33] I. M. Bullock, J. Z. Zheng, S. D. L. Rosa, C. Guertler, and A. M. Dollar, "Grasp frequency and usage in daily household and machine shop tasks," *IEEE Trans. Haptics*, vol. 6, no. 3, pp. 296–308, Jul./Sep. 2013.
[34] K. Deb, A. Pratap, S. Agarwal, and T. Meyarivan, "A fast and elitist multiobjective genetic algorithm: NSGA-II," *IEEE Trans. Evol. Comput.*, vol. 6, no. 2, pp. 182–197, Apr. 2002.
[35] N. Hogan, "Impedance control: An approach to manipulation: Part I-theory. Part II-Implementation. Part III-Applications," *J. Dyn. Syst. Meas. Control*, vol. 107, no. 1, pp. 1–24, 1985.
[36] H. Li, L. Cheng, Z. Li, and G. Li, "UCAS-Hand: An underactuated powered hand exoskeleton for assisting grasping task," in *Proc. IEEE Int. Conf. Real-time Comput. Robot.*, 2021, pp. 1–6.

Houcheng Li received the B.E. degree in control engineering from the Beijing University of Posts and Telecommunications, Beijing, China, in 2017. He is currently working toward the Ph.D. degree in control theory and control engineering with the State Key Laboratory of Management and Control for Complex Systems, Institute of Automation, Chinese Academy of Sciences, Beijing, China.

His research interests include rehabilitation robot control, robot system design, and human-robot interaction.

Long Cheng (Senior Member, IEEE) received the B.S. (Hons.) degree in control engineering from Nankai University, Tianjin, China, in 2004, and the Ph.D. (Hons.) degree in control theory and control engineering from the Institute of Automation, Chinese Academy of Sciences, Beijing, China, in 2009.

He is currently a Full Professor with the Institute of Automation, Chinese Academy of Sciences. He is also an Adjunct Professor with the University of Chinese Academy of Sciences, Beijing, China. He has authored and coauthored more than 100 technical papers in peer-refereed journals and prestigious conference proceedings. His research interests include the rehabilitation robot, intelligent control, and neural networks.

Dr. Cheng was the recipient of the IEEE TRANSACTIONS ON NEURAL NETWORKS Outstanding Paper Award from IEEE Computational Intelligence Society, the Aharon Katzir Young Investigator Award from International Neural Networks Society, and the Young Researcher Award from Asian Pacific Neural Networks Society. He is currently an Associate Editor/Editorial Board Member of IEEE TRANSACTIONS ON CYBERNETICS, *Neural Processing Letters*, *Neurocomputing*, *International Journal of Systems Science*, and *Acta Automatica Sinica*.

Ning Sun received the B.E. degree in mechanical engineering from the Qingdao University, Qingdao, China, in 2015, and the M.S. degree in mechanical engineering from the Beijing Institute of Technology, Beijing, China, in 2018. He is currently working toward the Ph.D. degree in control theory and control engineering with the State Key Laboratory of Management and Control for Complex Systems, Institute of Automation, Chinese Academy of Sciences, Beijing, China.

His research interests include rehabilitation robot design and compliant actuator technology.

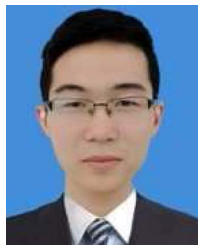

Ran Cao received the B.E. degree in control engineering from the Harbin Engineering University, Harbin, China, in 2015, the M.S. degree in control engineering from the Harbin Institute of Technology, Shenzhen, Guangdong, China, in 2018. He is currently working toward the Ph.D. degree in computer applied technology with the School of Artificial Intelligence, University of Chinese Academy of Sciences, Beijing, China.

He is with the Institute of Automation, Chinese Academy of Sciences, Beijing, China. His research interests include human-robot interaction and robot learning.